Damage Identification in Composite Beam by Vibration Measurement and Fuzzy Inference System

Irshad Ahmad Khan[*]**, Dayal Ramakrushna Parhi**[*]

Department of Mechanical Engineering, National Institute of Technology, Rourkela, India
*Corresponding author: irshadak85@gmail.com, drkparhi@nitrkl.ac.in

Abstract A significant efforts have been done by scientists and researchers in the last few years to develop many non-destructive techniques for damage recognition in a beam like dynamic structures. In this paper, theoretical, numerical, fuzzy logic methods employed for diagnosis of damage in the form of cracks of the cantilever composite beam with an aim to detect, quantify, and determine its intensity and locations. The Glass fiber reinforced epoxy composite engaged in the analysis due to high strength and stiffness-to-weight ratios. The theoretical analysis is performed to get the relationship between change in natural frequencies and mode shapes for the cracked and non-cracked composite beam. The Numerical analysis is performed on the cracked composite beam to get the vibration parameters such as natural frequency and mode shape, which is used to design fuzzy logic, based smart artificial intelligent technique for predicting crack severity and its intensity. Online fuzzy based smart technique has been developed, first three natural frequencies and mode shapes used as input parameters, Gaussian membership functions is considered to detect cracks location and depth. The results of theoretical and numerical analysis are compared with experimental results having good agreement with the results predicted by the fuzzy inference system.

Keywords: *vibration, fuzzy, natural frequency, mode shape, ansys, crack, composite beam*

Cite This Article: Irshad Ahmad Khan, and Dayal Ramakrushna Parhi, "Damage Identification in Composite Beam by Vibration Measurement and Fuzzy Inference System." *Journal of Mechanical Design and Vibration*, vol. 3, no. 1 (2015): 8-23. doi: 10.12691/jmdv-3-1-2.

1. Introduction

The demand for composite materials is increasing, especially in the aerospace, civil and automobile industries, due to its unique characteristics such as high stiffness and strength to weight ratio, higher fatigue and wear resistance and higher damage tolerance capability. Sometimes composite and isotropic structures subjected to dynamic loading, which is one of the causes of damage mostly, cracks and delamination. The presence of the cracks on the dynamic structures introduces a local flexibility, which changes the dynamic behavior of the structures.

For the last few years, several methodologies have been explored for monitoring and detection of the damage in the composite materials. Kisa [1] has developed a new numerical method for free vibration analysis of cracked cantilever composite beam having multiple transverse cracks. The proposed method integrates the fracture mechanics and the joint interface mechanics to couple substructures. Kisa et al. [2] are presented a new numerical methodology for free vibration analysis of circular cross sectional beams containing multiple non-propagating open cracks. In the proposed methodology the component mode synthesis technique is combined with the finite element method. Krawczuk et al. [3] are presented two models to calculate Eigen frequencies of cracked graphite fiber reinforced polyimide composite

beam. In the first model the crack is exhibited by a mass-less substitute spring. The fracture mechanics and the Castigliano theorem are used to calculate the flexibility of the spring. The finite element method is utilized in the second model. Hoffman et al. [4] are presents three neural classification methodologies were calculated from their performance on a fault diagnosis problem needful for the multiple fault identification. Adams et al. [5] propose a non-destructive method for evaluating the integrity of structures. Crack location and crack depth identified by proposed theoretical method and justified by experimental investigation. Sekhar [6] is determined dynamic characteristics of cracked rotor containing two cracks through finite element analysis and the influence of one crack over the other for natural frequencies, mode shapes and for threshold speed limits has been observed. Pawar et al. [7] are developed online damage detection method for composite rotor blade. Finite element method used to obtain system parameters such as blade response, loads and strains of the damage and un-damage rotor blade, these parameters used as input to genetic fuzzy systems for identification of damage in the rotor blade. Katunin [8] is presented discrete wavelet transform method for identification of multiple cracks on polymeric laminate beam. The natural mode shapes of non-cracked and cracked beams were estimated experimentally using laser Doppler vibrometry for estimation of the crack locations in laminated beams. Saravanan et al. [9] have proposed a method based on the vibration signatures acquired from

the machines to effectively identify the conditions of remote moving parts of the machine. The proposed method has been designed using fuzzy controller and decision trees to produce the rules automatically from the feature set. The developed fuzzy controller has been tested with characteristic data and the results are found to be inspiring. Das et al. [10] are presented finite element, theoretical, experimental and fuzzy logic methodologies for forecasting the crack severity and its intensity on beam. Finite element analysis is being executed on the cracked beam structure to measure the vibration parameters, which is subsequently used in the fuzzy logic controller for prediction of crack depths and locations. Results from experimental analysis are very close to the results predicted by the theoretical, finite element and fuzzy analysis. Parhi [11] has developed a fuzzy based navigational control system for multiple mobile robots working in a cluttered environment. He has been designed to navigate in cluttered environment without hitting any obstacles along with other robots. Mohammed et al. [12] are proposed a neuro-fuzzy system for identification of multiple damage in pre-stressed square membrane structure. The neuro-fuzzy system receives the wavelet-based damage feature index vector as the input and gives the damage status of the structure as the output. In the present work, the artificial intelligent technique has been adopted for the identification of cracks. Theoretical and numerical have been performed to find the dynamic response of a cracked cantilever composite. The theoretical and numerical results have been compared. An inverse method has been designed based on fuzzy technique with Gaussian membership function and used to forecast the damage severity and its intensity. The experiment results are compared with the various analysis results. A close agreement observed between the results.

2. Theoretical Analysis of Cracked Composite Beam

2.1. Stiffness and Mass Matrices for Composite Beam Element

The method suggested by Krawczuk [3] can be used to find the stiffness and mass matrices of the composite beam element and assume to three nodes in an element, one node in the middle and two at the extreme end of an element, and three degrees of freedom at each node is, $\delta = \{u, v, \theta\}$ shown in fig , the applied system forces F= {F_1, S_1, M_1, F_2, S_2, M_2, F_3, S_3, M_3} and corresponding displacements $\delta = \{u_1, v_1, \theta_1, u_2, v_2, \theta_2, u_3, v_3, \theta_3\}$ are shown in Figure 2. The stiffness matrix for a three-node composite beam element with three degrees of freedom at each node, for case of bending in x-y plane, given as follows [3].
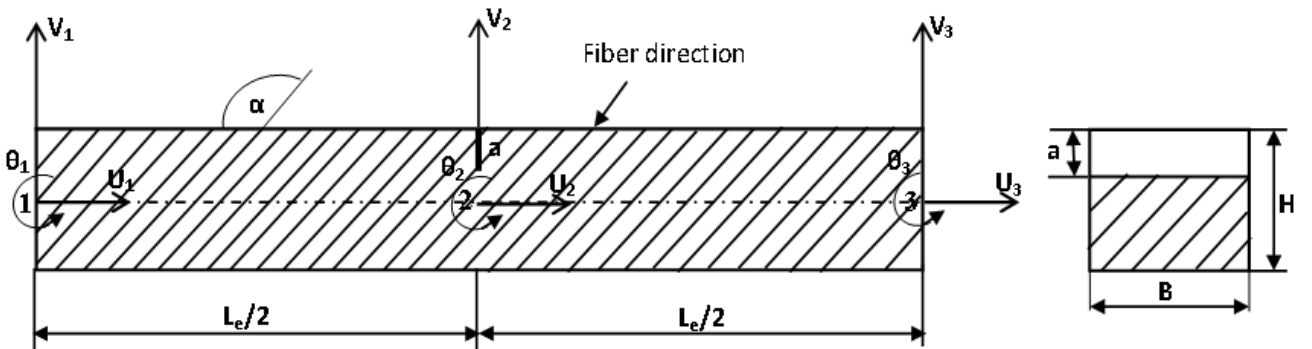

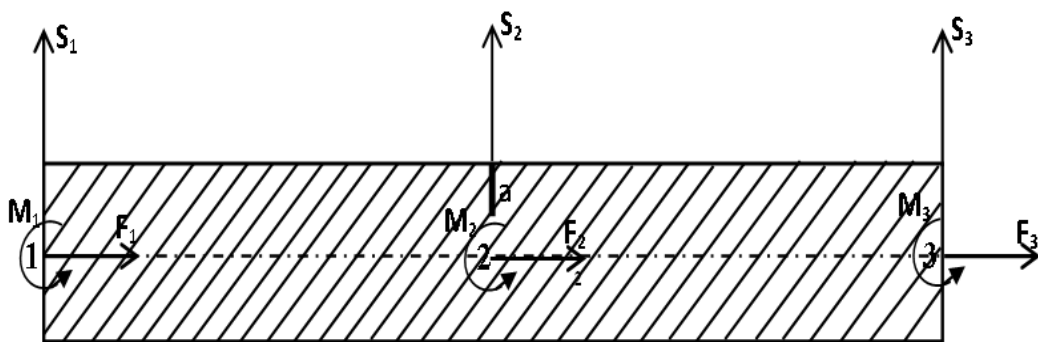**Figure 1.** Nodal displacement in element coordinate system

Figure 2. Applied forces on beam element

$$K_{el} = \left[q_{ij} \right]_{(9\times9)} \qquad (1)$$

Where $q_{ij}(i, j=1\dots 9)$ are shown in Appendix A.

The mass matrix of the composite beam element can be given as [3]

$$M_{el} = \left[M_{ij} \right]_{(9\times9)}, \qquad (2)$$

Where $M_{ij}(i, j=1\dots 9)$ are shown in Appendix B.

2.2. The Determination of Stiffness Matrix for the Cracked Composite Beam Element

According to the St. Venant's principle, the stress field is influenced only in the vicinity of the crack. The additional strain energy generates due to crack, which

change flexibility coefficients expressed by stress intensity factors, can be derived by Castigliano's theorem in the linear elastic range. In this study, the bending-stretching effect due to mid-plane asymmetry encouraged by the cracks is neglected. The coefficients of compliance C_{ij} are derived from the strain energy release rate (J), which induced by cracks developed by Griffith–Irwin theory [16]. J can be expressed as

$$j = \frac{\partial U\left(P_i, A\right)}{\partial A} \tag{3}$$

Where A = area of the crack section, P_i = corresponding loads, U = strain energy of the beam due to presence of crack and can be written as [15]

$$U = \int_A \begin{pmatrix} D_1 \sum_{i=1}^{i=N} K_{Ii}^2 + D_{12} \sum_{i=1}^{i=N} K_{Ii} \sum_{j=1}^{j=N} K_{IIj} \\ + D_2 \sum_{i=1}^{i=N} K_{IIi}^2 + D_3 \sum_{i=1}^{i=N} K_{IIIi}^2 \end{pmatrix} dA, \tag{4}$$

Where: K_I, K_{II} and K_{III} are the stress intensity factors for fracture modes of opening, sliding and tearing type of crack. D_1, D_{12}, D_2 and D_3 are the coefficients depending on the material parameters [13]

$$\left.\begin{aligned} D_1 &= -0.5\overline{d}_{22}\mathrm{Im}(\frac{s_1 + s_2}{s_1 s_2}), \\ D_{12} &= \overline{d}_{11}\mathrm{Im}(s_1 s_2), \\ D_2 &= 0.5\overline{d}_{11}\mathrm{Im}(s_1 + s_2), \\ D_3 &= 0.5\ \overline{d}_{44}\ \overline{d}_{55} \end{aligned}\right\} \tag{5}$$

The coefficients s_1, s_2 and d_{ij} are given in Appendix C. The stress intensity factors, K_I, K_{II} and K_{III} expressed as [14]:

$$K_{ji} = \sigma_i \sqrt{\pi a}\, Y_j(\xi) F_{ji}(a/H), \tag{6}$$

Where σ_i = stress for the corresponding fracture mode, $F_{ji}(a/H)$ = correction factor for the finite specimen size; $Y_j(\xi)$, = correction factor for the anisotropic material [13], a = crack depth and H = element height. Additional displacement due to crack, according to the Castigliano's theorem [17], in the direction of the load P_i, is

$$u_i = \frac{\partial U(P_i, A)}{\partial P_i}. \tag{7}$$

Substituting the Eq. (3) into Eq. (7), displacement and strain energy release rate J can be related as follows:

$$u_i = \frac{\partial}{\partial P_i} \int_A J(P_i, A) dA, \tag{8}$$
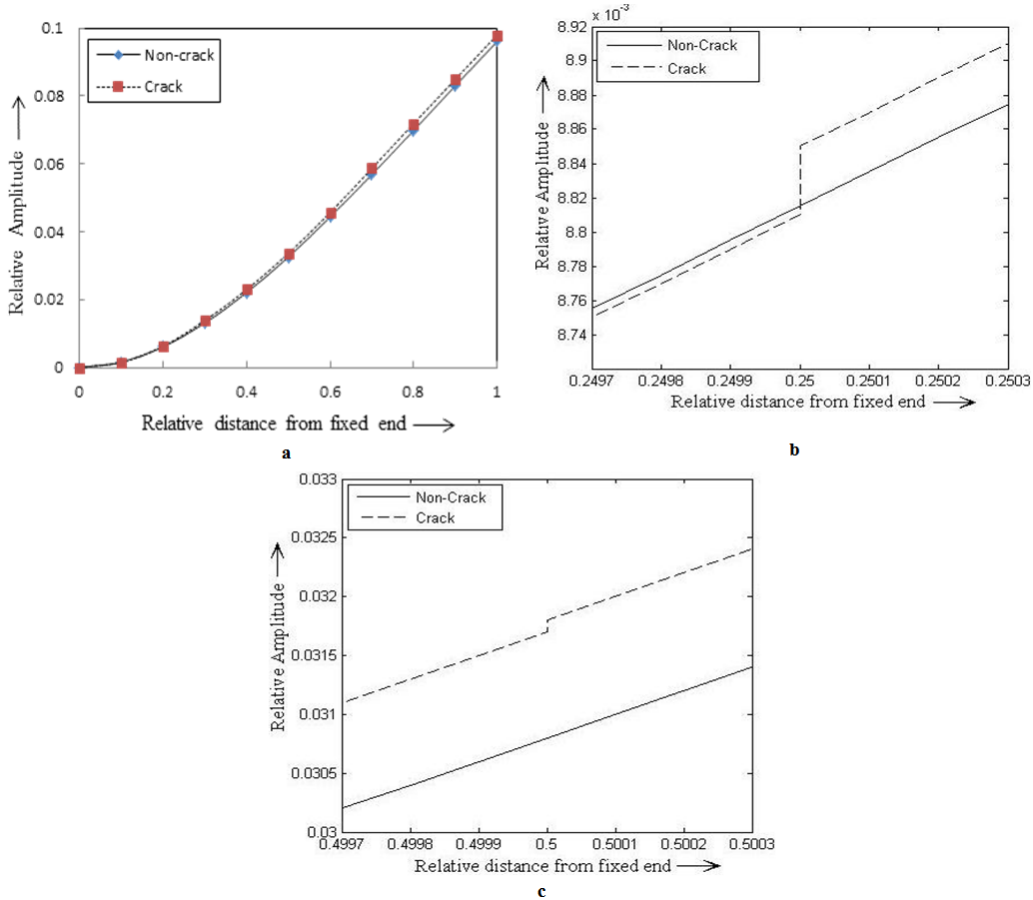
Figure 3. a Relative Amplitude vs. Relative distance from fixed end (1st mode of vibration), **b** Magnified view at the first crack location (β_1=0.25), **c** Magnified view at the second crack location (β_1=0.5)

The flexibility coefficients, which are highly depend on the stress intensity factors and the shape and size of crack and, can be written as [16]:

$$c_{ij} = \frac{\partial u_i}{\partial P_j} = \frac{\partial^2}{\partial P_i \partial P_j} \int_A J(P_i, A) dA = \frac{\partial^2 U}{\partial P_i \partial P_j}, \tag{9}$$

The compliance coefficient matrix, can be derived from the above equation, can be assumed according to the displacement vector $\delta = \{u, v, \theta\}$ as

$$C = \left[c_{ij} \right]_{(6 \times 6)} \quad (10)$$

Where c_{ij} (i, j=1 to 6) are derived by using eqs. (3)- (9).

The matrix of transformation [T] is calculated by using the equation of overall equilibrium of elemental forces (Fi = 1, 9) and (Si = 1, 6). The final matrix of transformation is

$$[T]^t = \begin{bmatrix} 1 & 0 & 0 & 0 & 0 & 0 \\ 0 & 1 & 0 & 0 & 0 & 0 \\ 0 & 0 & 1 & 0 & 0 & 0 \\ -1 & 0 & 0 & -1 & 0 & 0 \\ 0 & -1 & 0 & 0 & -1 & 0 \\ 0 & L_e/2 & -1 & 0 & L_e/2 & -1 \\ 0 & 0 & 0 & 1 & 0 & 0 \\ 0 & 0 & 0 & 0 & 1 & 0 \\ 0 & 0 & 0 & 0 & 0 & 1 \end{bmatrix} \quad (11)$$
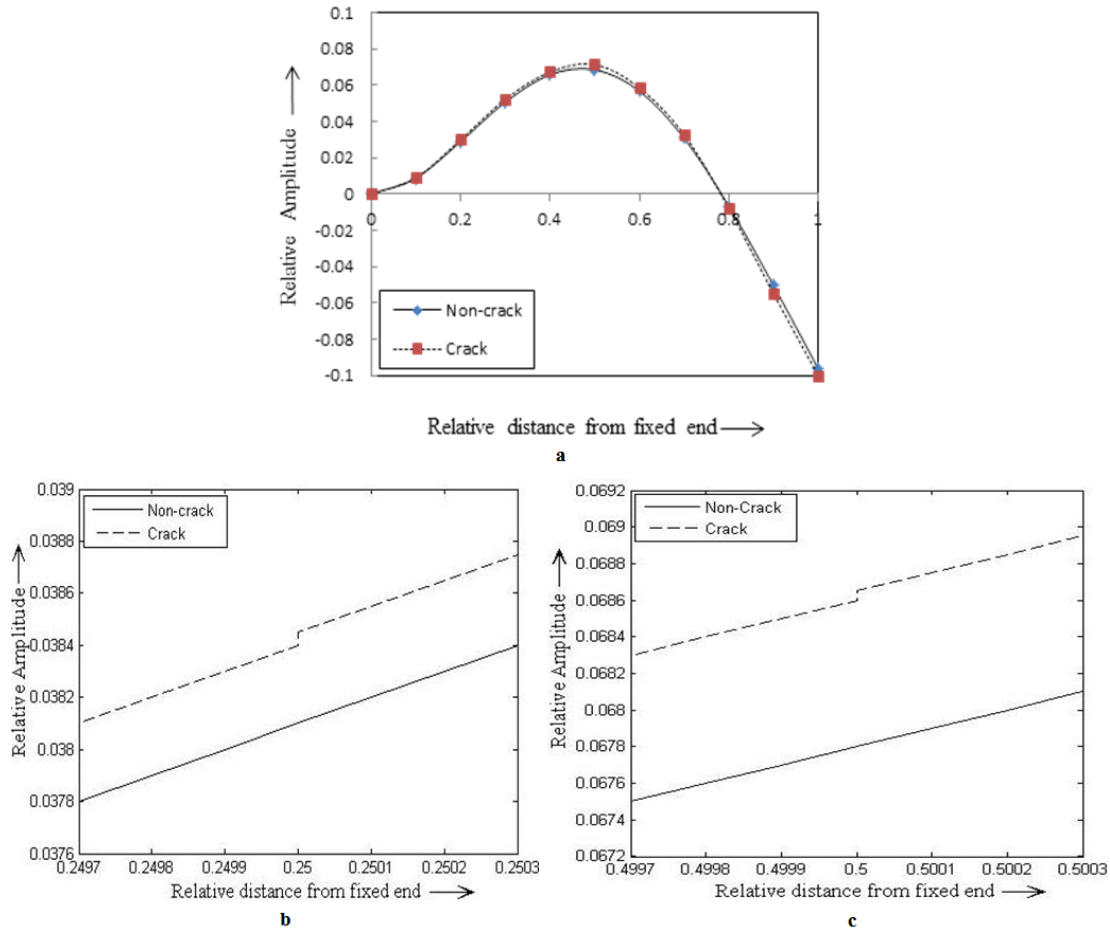
Figure 4. a Relative Amplitude vs. Relative distance from fixed end (2ndmode of vibration), **b** Magnified view at the first crack location (β$_1$=0.25), **c** Magnified view at the second crack location (β$_1$=0.5)

Hence the stiffness matrix of a cracked beam element can be obtained as

$$K_{Crack} = TC^{-1}T^t \quad (12)$$

Natural frequencies are calculated by following equation [21]

$$w_n = \alpha^2 \left(\frac{IS_{11}}{\rho A L_e^4} \right)^{1/2} \quad (13)$$

Where α^2 is the co-efficient, which value is catalogued by Warburton, Young and Felgar.

The theoretical analysis results for the first three mode shapes for non-cracked and cracked composite beam are shown in Figure 3, Figure 4, and Figure 5 and the orientation of the cracks are β$_1$=0.25, β$_2$=0.5, ψ$_1$=0.1667 and ψ$_2$=0.5. Magnified view at the vicinity of the first and

second crack for first three mode of vibration are shown in Figure 3b, Figure 3c, Figure 4b, Figure 4c, Figure5b and Figure 5c. A sudden jump has been observed in relative amplitudes; these changes in amplitudes will be helpful in the prediction of crack location and its intensity.

3. Numerical Analysis of Cracked Composite Beam

The numerical analysis is brought out for the cracked cantilever composite beam shown in Figure 6, to find the vibration signatures, e.g. natural frequencies and mode shapes of transverse vibration at different crack depth and crack location. The individual material properties of fiber and matrix listed in Table 1. The cracked beams of the current research have the following dimensions.
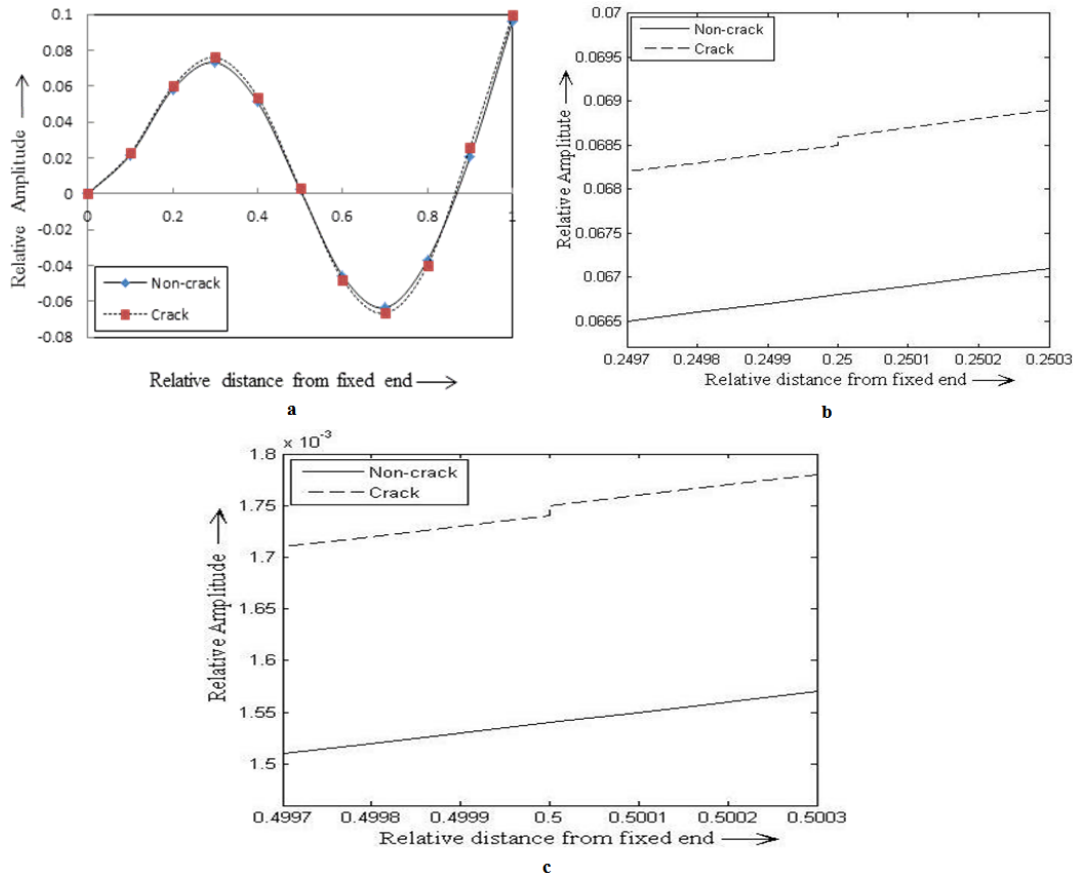
Figure 5. a Relative Amplitude vs. Relative distance from fixed end (3rd mode of vibration), **b** Magnified view at the first crack location (β_1=0.25), **c** Magnified view at the second crack location (β_1=0.5)
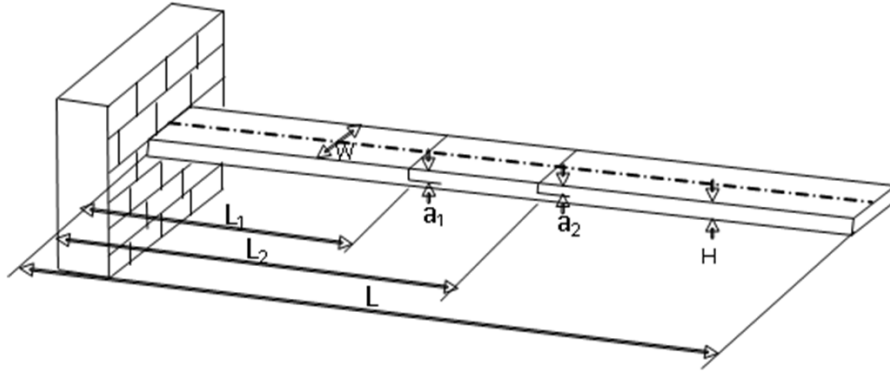
Figure 6. Geometry Cracked Cantilever beam
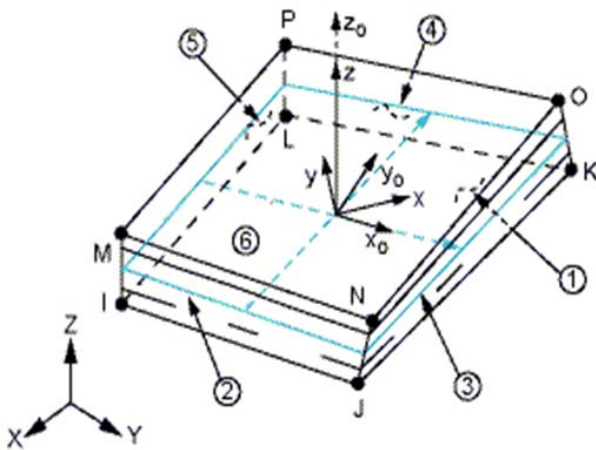
**Figure 7.** Geometry of Structural Solid Shell (SOLSH190) element

Table 1. Properties of Glass fiber- reinforced epoxy composite

	Fiber (Glass)	Matrix (Epoxy)
Elastic Modulus (Gpa)	$E_f = 72.4$	$E_m = 3.45$
Rigidity Modulus (Gpa)	$G_f = 29.67$	$G_m = 1.277$
Poisson's Ratio	$\upsilon_f = 0.22$	$\upsilon_m = 0.35$
Mass Density (gm-cm^{-3})	$\rho_f = 2.6$	$\rho_m = 1.2$

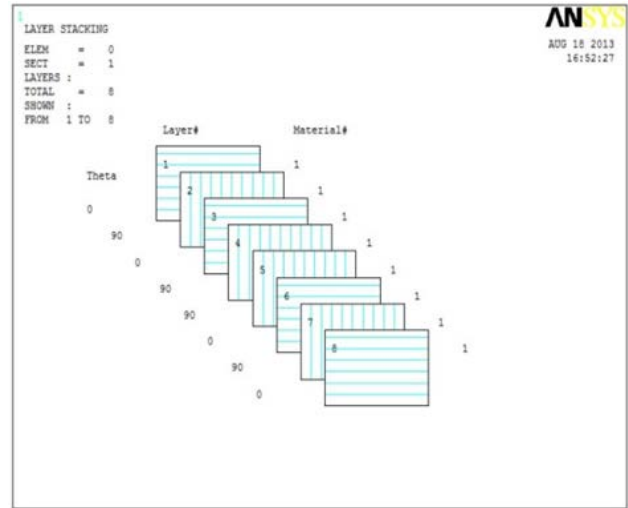Length of the Beam (L) = 800mm; Width of the beam (W) = 50mm; Thickness of the Beam (H) = 6mm

1. Relative first crack depth ($\psi_1 = a_1/H$) varies from 0.0833 to 0.5;
2. Relative second crack depth ($\psi_2 = a_2/H$) varies from 0.0833 to 0.5;
3. Relative first crack location ($\beta_1 = L_1/L$) varies from 0.0625 to 0.875;
4. Relative second crack location ($\beta_2 = L_2/L$) varies from 0.125 to 0.9375;
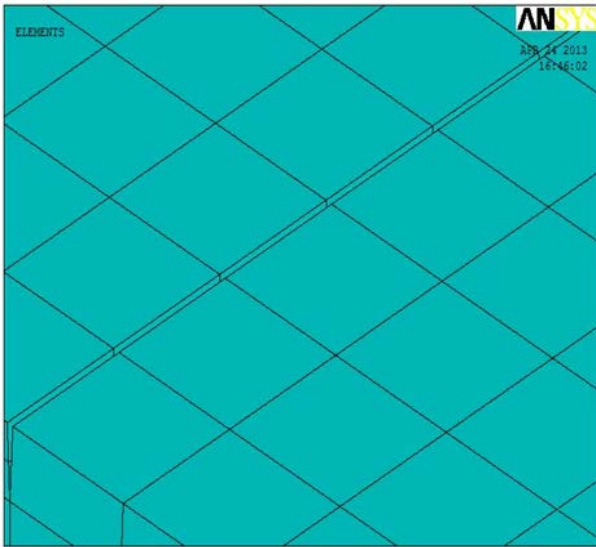
Figure 8. Meshing at the vicinity of crack

Figure 9. Layers Stacking in ANSYS

Numerical modal analysis based on the finite element modeling is performed for studying the dynamic response of a dynamic structure. The natural frequencies and mode shapes are most important modal parameters in designing a structure under complex loading conditions. The numerical analysis is accepted by using the finite element software ANSYS in the frequency domain and obtain natural frequencies, and mode shapes.

A higher order 3-D, 8-node element (Specified as SOLSH190 in ANSYS) having three degrees of freedom at each node: translations in the nodal x, y, and z directions is selected and used throughout the analysis shown in Figure 7. Each node has three degrees of freedom, making a total twenty four degrees of freedom per element. The hexagonal meshing at the vicinity of crack is shown in Figure 8. The layers, stacking of composite beam is in the ANSYS shown in Figure 9.

a

b

c
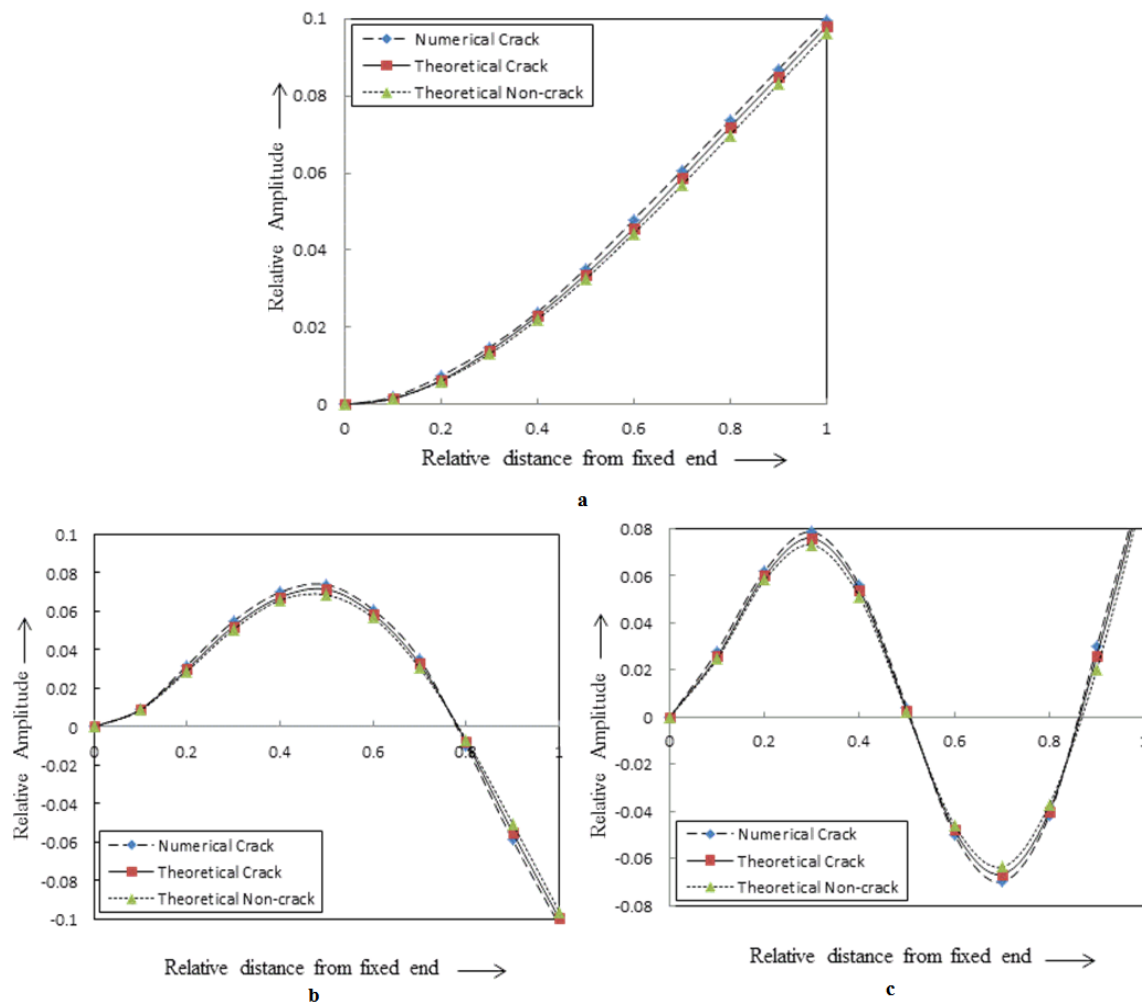
Figure 10. a Relative Amplitude vs. Relative distance from fixed end (1st mode of vibration), **b** Relative Amplitude vs. Relative distance from fixed end (2nd mode of vibration)**, c** Relative Amplitude vs. Relative distance from fixed end (3rd mode of vibration)

The results of numerical analysis for the first three mode shapes for cracked composite beam plotted along with theoretical analysis results for cracked and non-cracked beam, orientation of cracks (β_1=0.25, β_2=0.5, ψ_1=0.1667 and ψ_2=0.5) is shown in the Figure 10.

4. Fuzzy Logic Analysis for Identification of Cracks

The fuzzy controller has developed having six input parameters and two output parameters as shown in Figure 11. The linguistic term used for the inputs are as follows; Relative first natural frequency = "rfnf"; Relative second natural frequency = "rsnf"; Relative third natural frequency = "rtnf"; Relative first mode shape difference = "rfmd"; Relative second mode shape difference = "rsmd"; Relative third mode shape difference = "rtmd.

The linguistic term used for the outputs are as follows; Relative first crack location = "rfcl" Relative second crack location = "rscl" Relative first crack depth = "rfcd" Relative second crack depth = "rscd".
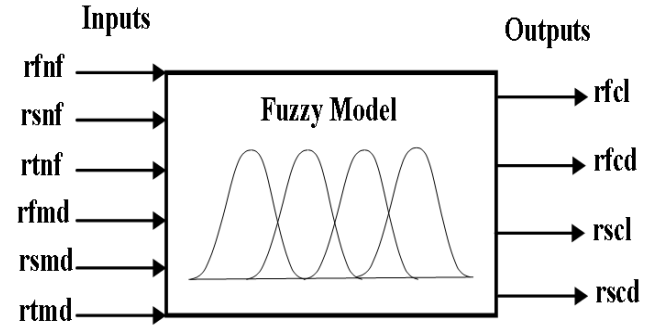

Figure 11. Gaussian fuzzy model

The membership functions for linguistic terms, used in fuzzy inference system shown in Figure 13 and described in Table 2.
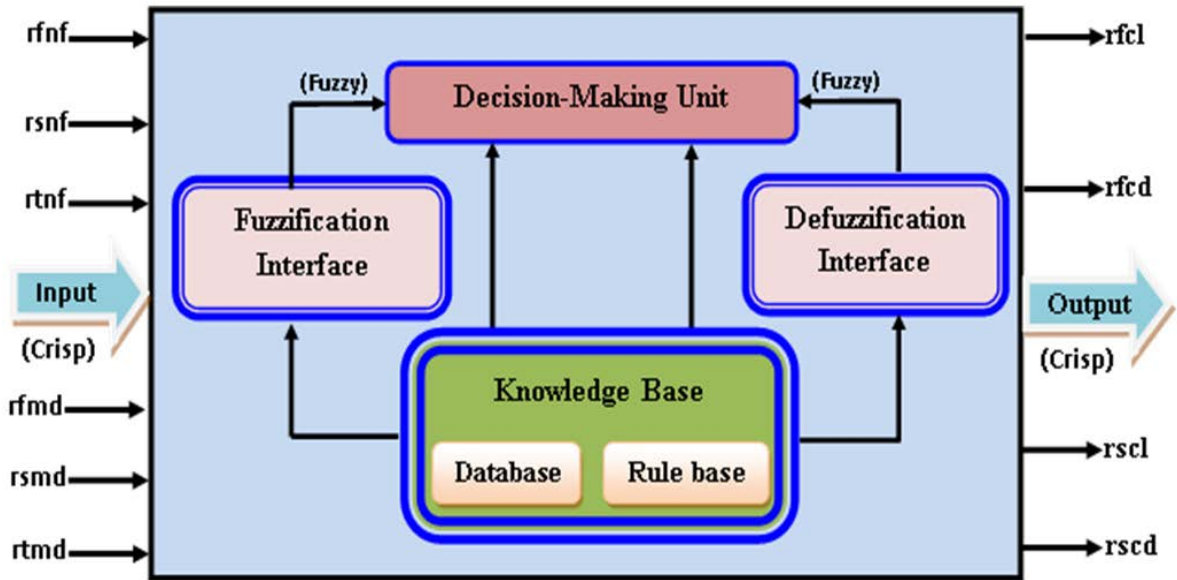

Figure 12. Fuzzy inference system

4.1. Fuzzy Tools for Identification of Crack

The rules for fuzzy mechanism can be defined, based on above fuzzy linguistic terms as follow:

$$\text{if} \begin{pmatrix} \text{rfnf is rfnf}_a \text{ and rsnf is rsnf}_b \\ \text{and rtnf is rtnf}_c \quad \text{rfmd is rfmd}_e \\ \text{and rsmd is rsmd}_f \text{ and rtmd is rtmd}_g \end{pmatrix} \tag{14}$$

then rfcl is rfcl$_{abcefg}$ and rfcd is rfcd$_{abcefg}$

and rscl is rscl$_{abcefg}$ and rscd is rscd$_{abcefg}$

where a, b, c, e, f, g = 1 to 12

According to fuzzy methodology a factor, W$_{abcefg}$ is defined in the rules as follows [11]

$$W_{abcefg} = \mu \, \text{rfnf}_a \left(\text{freq}_a\right) \wedge \mu \, \text{rsnf}_a \left(\text{freq}_b\right)$$
$$\wedge \mu \, \text{rtnf}_a \left(\text{freq}_c\right) \wedge \mu \, \text{rfmd}_e \left(\text{modshdif}_e\right) \tag{15}$$
$$\wedge \mu \, \text{rsmd}_f \left(\text{modshdif}_f\right) \wedge \mu \, \text{rtmd}_g \left(\text{modshdif}_g\right)$$

Where freq_a, freq_b and freq_c are the first, second and third relative natural frequencies of the cracked cantilever composite beam respectively; modshdif_e, modshdif_f and modshdif_g average relative mode shape differences of the cracked cantilever composite beam. The membership values of the relative crack location and relative crack depth, (location)$_{rcli}$and (depth) $_{rcdi}$ (i= 1, 2) by applying the composition rule of inference can be written as [11];

$$\mu_{rcli_{abcefg}} \text{(location)}$$
$$= w_{abcefg} \wedge \mu_{rcli_{abcefg}} \text{(location)} \, \forall_{length} \in \text{rcli}$$
$$\mu_{rcdi_{abcefg}} \text{(depth)} \tag{16}$$
$$= w_{abcefg} \wedge \mu_{rcdi_{abcefg}} \text{(depth)} \qquad \forall_{depth} \in \text{rcdi}$$

The outputs of all the fuzzy set rules combined to achieve the inclusive conclusions can be written as follows;

$$\mu_{\text{rcli}} (\text{location}) = \mu_{\text{rcli}_{11111}} (\text{location}) \lor .....$$

$$\lor \mu_{\text{rcli}_{\text{abcefg}}} (\text{location}) \lor .....$$

$$\lor \mu_{\text{rcli}_{121212121212}} (\text{location}) \tag{17}$$

$$\mu_{\text{rcli}} (\text{depth}) = \mu_{\text{rcli}_{11111}} (\text{depth}) \lor .....$$

$$\lor \mu_{\text{rcli}_{\text{abcefg}}} (\text{depth}) \lor ..... \lor \mu_{\text{rcli}_{121212121212}} (\text{depth})$$

The crisp values of the relative crack location and relative crack depth can be written with the help Centre of gravity method as [11]:

$$\left. \begin{array}{l} \text{Relative crack location (rfcl, rscl)} \\ \\ = \dfrac{\int (\text{location}) \cdot \mu_{\text{rcl}_{1,2}} (\text{location}) \cdot d\,(\text{location})}{\int \mu_{\text{rcl}_{1,2}} (\text{location}) \cdot d\,(\text{location})} \\ \\ \text{Relative crack depth (rfcd, rscd)} \\ \\ = \dfrac{\int (\text{depth}) \cdot \mu_{\text{rcl}_{1,2}} (\text{depth}) \cdot d\,(\text{depth})}{\int \mu_{\text{rcl}_{1,2}} (\text{depth}) \cdot d\,(\text{depth})} \end{array} \right\} \tag{18}$$
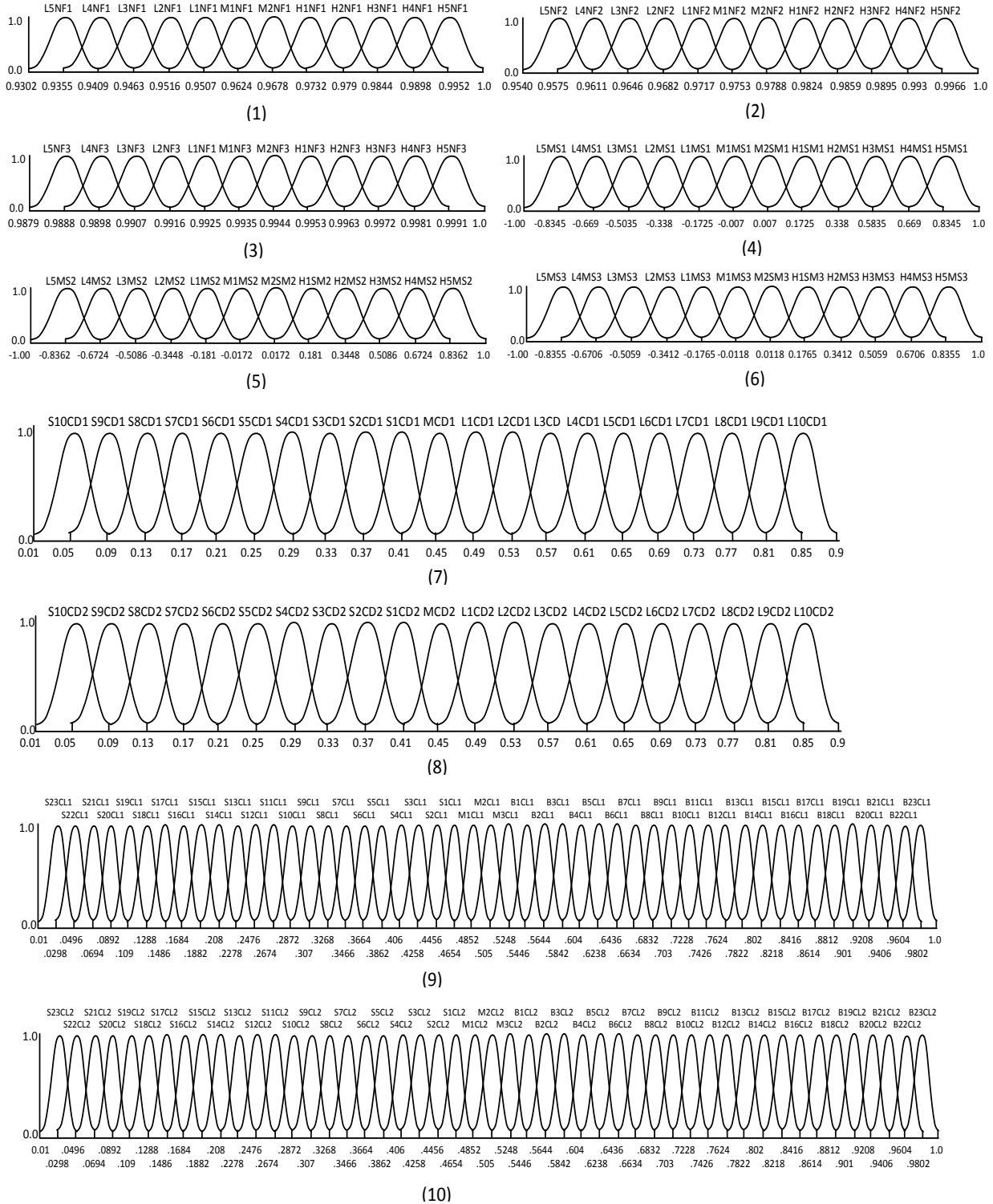
Figure 13. Fuzzy membership functions for (1, 2, 3) relative natural frequency of first three bending mode of vibration, (4, 5, 6) relative mode shape difference of first three bending mode of vibration, (7, 8) first and second crack depth and (9, 10) first and second crack location

Table 2. Description of fuzzy linguistic terms.

Membership Functions	Linguistic Terms	Description of the Linguistic terms
L1NF1, L2NF1, L3NF1, L4NF1, L5NF1	$rfnf_{1-5}$	Low ranges of relative natural frequency of the first mode of vibration in descending order respectively
M1NF1, M2NF1	$rfnf_{6,7}$	Medium ranges of relative natural frequency of the first mode of vibration in ascending order respectively
H1NF1, H2NF1, H3NF1, H4NF1, H5NF1	$rfnf_{8-12}$	Higher ranges of relative natural frequency of the first mode of vibration in ascending order respectively
L1NF2, L2NF2, L3NF2, L4NF2, L5NF2	$rsnf_{1-5}$	Low ranges of relative natural frequency of the second mode of vibration in descending order respectively
M1NF2, M2NF2	$rsnf_{6,7}$	Medium ranges of relative natural frequency of the second mode of vibration in ascending order respectively
H1NF2, H2NF2, H3NF2, H4NF2, H5NF2	$rsnf_{8-12}$	Higher ranges of relative natural frequencies of the second mode of vibration in ascending order respectively
L1NF3, L2NF3, L3NF3, L4NF3, L5NF3	$rtnf_{1-5}$	Low ranges of relative natural frequencies of the third mode of vibration in descending order respectively
M1NF3, M2NF3	$rtnf_{6,7}$	Medium ranges of relative natural frequencies of the third mode of vibration in ascending order respectively
H1NF3, H2NF3, H3NF3, H4NF3, H5NF3	$rtnf_{8-12}$	Higher ranges of relative natural frequencies of the third mode of vibration in ascending order respectively
S1MS1, S2MS1, S3MS1, S4MS1, S5MS1	$rfmd_{1-5}$	Small ranges of first relative mode shape difference in descending order respectively
M1MS1, M2MS1	$rfmd_{6,7}$	medium ranges of first relative mode shape difference in ascending order respectively
H1MS1, H2MS1, H3MS1, H4MS1, H5MS1	$rfmd_{8-12}$	Higher ranges of first relative mode shape difference in ascending order respectively
S1MS2, S2MS2, S3MS2, S4MS2, S5MS2	$rsmd_{1-5}$	Small ranges of second relative mode shape difference in descending order respectively
M1MS2, M2MS2	$rsmd_{6,7}$	medium ranges of second relative mode shape difference in ascending order respectively
H1MS2, H2MS2, H3MS2, H4MS2, H5MS2	$rsmd_{8-12}$	Higher ranges of second relative mode shape difference in ascending order respectively
S1MS3, S2MS3, S3MS3, S4MS3, S5MS3	$rtmd_{1-5}$	Small ranges of third relative mode shape difference in descending order respectively
M1MS3, M2MS3	$rtmd_{6,7}$	medium ranges of third relative mode shape difference in ascending order respectively
H1MS3, H2MS3, H3MS3, H4MS3, H5MS3	$rtmd_{8-12}$	Higher ranges of third relative mode shape difference in ascending order respectively
S1CL1, S2CL1……S23CL1	$rfcl_{1-23}$	Small ranges of relative first crack location in descending order respectively
M1CL1, M2CL1, M3CL1	$rfcl_{24-26}$	Medium ranges of relative first crack location in ascending order respectively
B1CL1, B2CL1…….B23CL1	$rfcl_{27-49}$	Bigger ranges of relative first crack location in ascending order respectively
S1CD1, S2CD1……S10CD1	$rfcd_{1-10}$	Small ranges of relative first crack depth in descending order respectively
MCD1	$rfcd_{11}$	Medium relative first crack depth
L1CD1, L2CD1……L10CD1	$rfcd_{12-21}$	Larger ranges of relative second crack depth in ascending order respectively
S1CL2, S2CL2……S23CL2	$rscl_{1-23}$	Small ranges of relative second crack location in descending order respectively
M1CL2, M2CL2, M3CL2	$rscl_{24-26}$	Medium ranges of relative second crack location in ascending order respectively
B1CL2, B2CL2…….B23CL2	$rscl_{27-49}$	Bigger ranges of relative second crack location in ascending order respectively
S1CD2, S2CD2……S10CD2	$rscd_{1-10}$	Small ranges of relative second crack depth in descending order respectively
MCD2	$rscd_{11}$	Medium relative second crack depth
L1CD2, L2CD2……L10CD2	$rscd_{12-21}$	Larger ranges of relative second crack depth in ascending order respectively

4.2. Fuzzy Controller for Detecting Crack Location and Crack Depth

Relative first natural frequency; relative second natural frequency; relative third natural frequency; average relative first mode shape difference; average relative second mode shape difference and average relative third mode shape difference are the input parameters for fuzzy controller. Relative first crack location; relative first crack depth; relative second crack location and relative second crack depth are the outputs from fuzzy controller. Twenty four numbers of fuzzy rules among several hundred rules are listed in Table 2. Figure 8 represents the fuzzy controller results when rule 6 and rule 16 are activated from Table 2.

5. Experimental Analyses

An experiment has been performed on cracked composite beam shown in Figure 11. Ten cracked composite beam specimens have been taken in experimental analysis with different crack location and depth. The composite beam was clamped on a vibrating table one by one. The cracked composite beams have been vibrated with the help of an exciter and a function generator. The vibration signatures such as natural frequencies and mode shapes of the composite beams correspond to 1st, 2nd and 3rd mode of vibration have been recorded by placing the accelerometer along the length of the beams and displayed on the vibration indicator. These results for first three mode shapes are plotted in Figure 12. Corresponding theoretical and numerical results for the cracked beam are also printed in the same graph for judgment. The name and description of instruments used in the analysis are listed in Table 3.
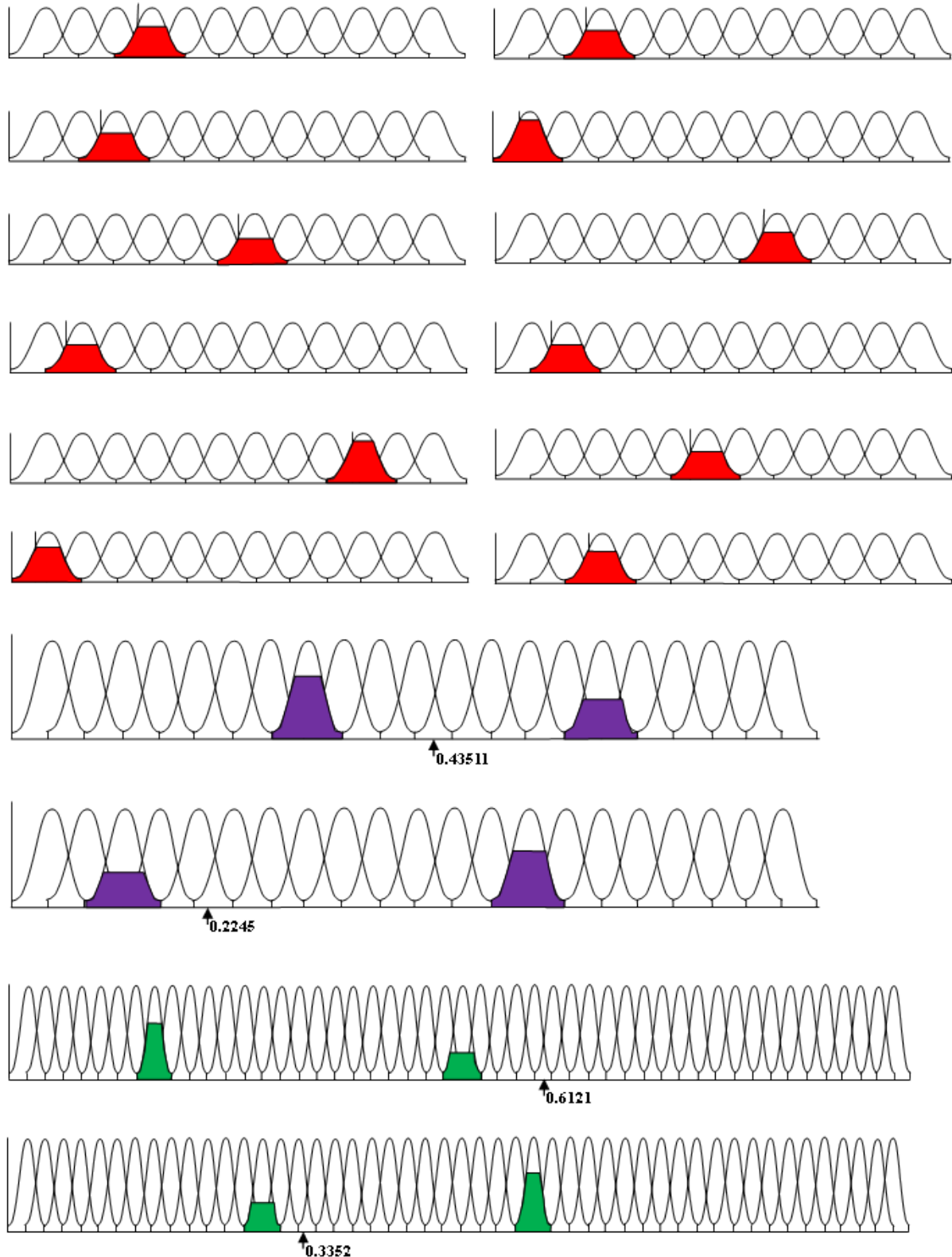

Figure 14. Resultant values of relative crack depths and relative crack locations when Rules 6 and 16 of Table 5.2 are activated

Table 3. Examples of twenty five fuzzy rules out of several hundred fuzzy rules

Sl. No.	Some rules for fuzzy controller
1	If rfnf is M1NF1,rsnf is L2NF2,rtnf is L1NF3,rfmd is M2MS1,rsmd is M2MS2,rtmd is H1MS3, then rfcd is S1CD1,and rfcl is S6CL1 and rscd is S4CD2,and rscl is B5CL2
2	If rfnf is M1NF1,rsnf is M1NF2,rtnf is M1NF3,rfmd is H3MS1,rsmd is H3MS2,rtmd is H4MS3, then rfcd is S6CD1,and rfcl is S18CL1 and rscd is S5CD2,and rscl is M2CL2
3	If rfnf is M1NF1,rsnf is L1NF2,rtnf is L1F3,rfmd is H3MS1,rsmd is H2MS2,rtmd is H3MS3, then rcd1 is S4CD1,and rfcl is S17CL1 and rscd is S6CD2,and rscl is B6CL2
4	If rfnf is M2NF1,rsnf is M1NF2,rtnf is M1NF3,rfmd is M1MS1,rsmd is H1MS2,rtmd is H2MS3, then rfcd is S4CD1,and rfcl is S11CL1 and rscd is S4CD2,and rscl is M2CL2
5	If rfnf is M1NF1,rsnf is L2NF2,rtnf is L3NF3,rfmd is H1MS1,rsmd is H1MS2,rtmd is H2MS3, then rfcd is S4CD1,and rfcl is S11CL1 and rscd is S1CD2,and rscl is B13CL2
6	If rfnf is L1NF4,rsnf is L2NF3,rtnf is M3NF2,rfmd is H2MS1,rsmd is H3MS2,rtmd is L1MS3, then rfcd is S3CD1,and rfcl is S16CL1 and rscd is S8CD2,and rscl is B3CL2
7	If rfnf is L4NF1,rsnf is L4NF2,rtnf is L4NF3,rfmd is M2MS1,rsmd is H1MS2,rtmd is H1MS3, then rfcd is L1CD1,and rfcl is S11CL1 and rscd is S4CD2,and rscl is B10CL2
8	If rfnf is H1NF1,rsnf is M2NF2,rtnf is M1NF3,rfmd is H2MS1,rsmd is H2MS2,rtmd is H2MS3, then rfcd is S6CD1,and rfcl is S6CL1 and rscd is S4CD2,and rscl is B5CL2
9	If rfnf is L1NF1,rsnf is L4NF2,rtnf is L4NF3,rfmd is M1MS1,rsmd is M1MS2,rtmd is M2MS3, then rfcd is S2CD1,and rfcl is S6CL1 and rscd is L1CD2,and rscl is B5CL2
10	If rfnf is H2NF1,rsnf is H1NF2,rtnf is H1NF3,rfmd is H4MS1,rsmd is H1MS2,rtmd is H1MS3, then rfcd is S7CD1,and rfcl is S17CL1 and rscd is S6CD2,and rscl is B16CL2
11	If rfnf is M1NF1,rsnf is L1NF2,rtnf is L2NF3,rfmd is S1MS1,rsmd is S2MS2,rtmd is H1MS3, then rfcd is S2CD1,and rfcl is S11CL1 and rscd is S6CD2,and rscl is B10CL2
12	If rfnf is L4NF1,rsnf is L4NF2,rtnf is L4NF3,rfmd is H2MS1,rsmd is S1MS2,rtmd is H2MS3, then rfcd is L1CD1,and rfcl is S17CL1 and rscd is S5CD2,and rscl is M2CL2
13	If rfnf is M1NF1,rsnf is L3NF2,rtnf is L1NF3,rfmd is S2MS1,rsmd is M1MS2,rtmd is S1MS3, then rfcd is S6D1,and rfcl is S12CL1 and rscd is MCD2,and rscl is M1CL2
14	If rfnf is L2NF1,rsnf is L1NF2,rtnf is L1NF3,rfmd is H2MS1,rsmd is H2MS2,rtmd is H2MS3, then rfcd is S2CD1,and rfcl is S12CL1 and rscd is S4CD2,and rscl is B13CL12
15	If rfnf is H2NF1,rsnf is H1NF2,rtnf is H1NF3,rfmd is S2MS1,rsmd is H3MS2,rtmd is H1MS3, then rfcd is S4CD1,and rfcl is S5CL1 and rscd is S6CD2,and rscl is B6CL2
16	If rfnf is L3NF1,rsnf is L1NF2,rtnf is H1NF3,rfmd is S2MS1,rsmd is M1MS2,rtmd is L3MS3, then rfcd is L5CD1,and rfcl is M2CL1 and rscd is L3CD2,and rscl is S10CL2
17	If rfnf is H1NF1,rsnf is M2NF2,rtnf is M1NF3,rfmd is H2MS1,rsmd is H4MS2,rtmd is H3MS3, then rfcd is S6CD1,and rfcl is S17CL1 and rscd is S4CD2,and rscl is S6CL2
18	If rfnf is L4NF1,rsnf is L4NF2,rtnf is L4NF3,rfmd is H1MS1,rsmd is H1MS2,rtmd is H2MS3, then rfcd is S2CD1,and the rifle is S17CL1 and rescued is S1CD2,and rscl is M2CL2
19	If rfnf is L3NF1,rsnf is L4NF2,rtnf is L4NF3,rfmd is M2MS1,rsmd is H2MS2,rtmd is H3MS3, then rfcd is MCD1,and rfcl is S17CL1 and rscd is S2CD2,and rscl is B19CL2
20	If rfnf is H2NF1,rsnf is H1NF2,rtnf is H1NF3,rfmd is H3MS1,rsmd is H4MS2,rtmd is H4MS3, then rfcd is S6CD1,and rfcl is S11CL1 and rscd is S4CD2,and rscl is M2CL2
21	If rfnf is H3NF1,rsnf is L2NF2,rtnf is M2NF3,rfmd is L2MS1,rsmd is H2MS2,rtmd is H1M3, then rfcd is S9CD1,and rfcl is S18CL1 and rscd is S11CD2,and rscl is S8CL2
22	If rfnf is M1NF1,rsnf is L3NF2,rtnf is H4NF3,rfmd is H2MS1,rsmd is S4MS2,rtmd is H3MS3, then rfcd is S12CD1,and rfcl is S18CL1 and rscd is S3CD2,and rscl is B10CL2
23	If rfnf is H3NF1,rsnf is M1NF2,rtnf is L1NF3,rfmd is M2MS1,rsmd is H3MS2,rtmd is H4MS3, then rfcd is MCD1,and rfcl is S14CL1 and rscd is S4CD2,and rscl is B14CL2
24	If rfnf is H4F1,rsnf is M1F2,rtnf is L4F3,rfmd is S4M1,rsmd is H1M2,rtmd is H4M3, then rfcd is S16CD1,and rfcl is B11L1 and rscd is M2CD2,and rscl is B2CL2
25	If rfnf is L3NF1,rsnf is L4NF5,rtnf is H2NF3,rfmd is S3MS4,rsmd is M1MS2,rtmd is H1MS3, then rfcd is L1CD3,and rfcl is S5CL1 and rscd is S2CD2,and rscl is B5CL2
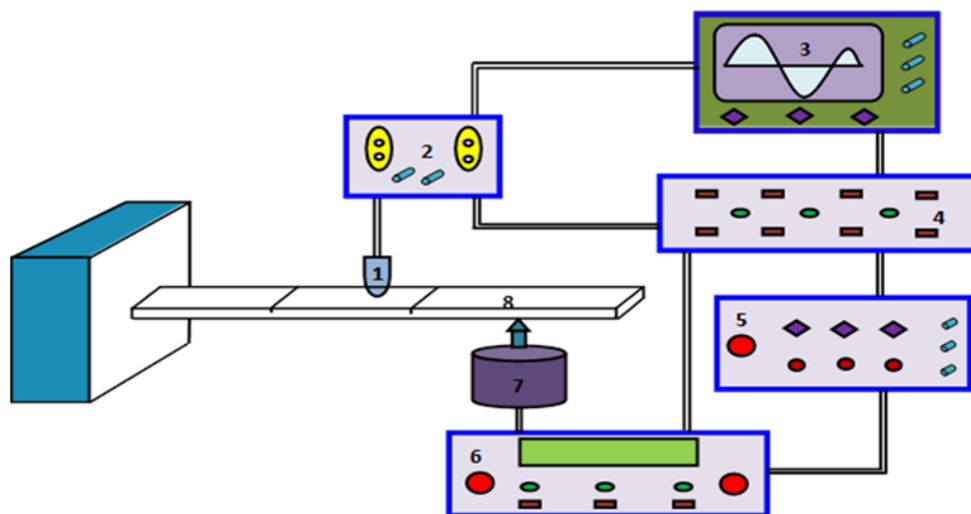
Figure 15. Schematic block diagram of experimental set-up

1. Delta tron Accelerometer; 2. Vibration analyzer; 3. Vibration indicator embedded with Pulse Lab shop software; 4. Power Distribution; 5. Function generator; 6. Power amplifier; 7. Vibration exciter; 8. Cracked Cantilever Composite beam
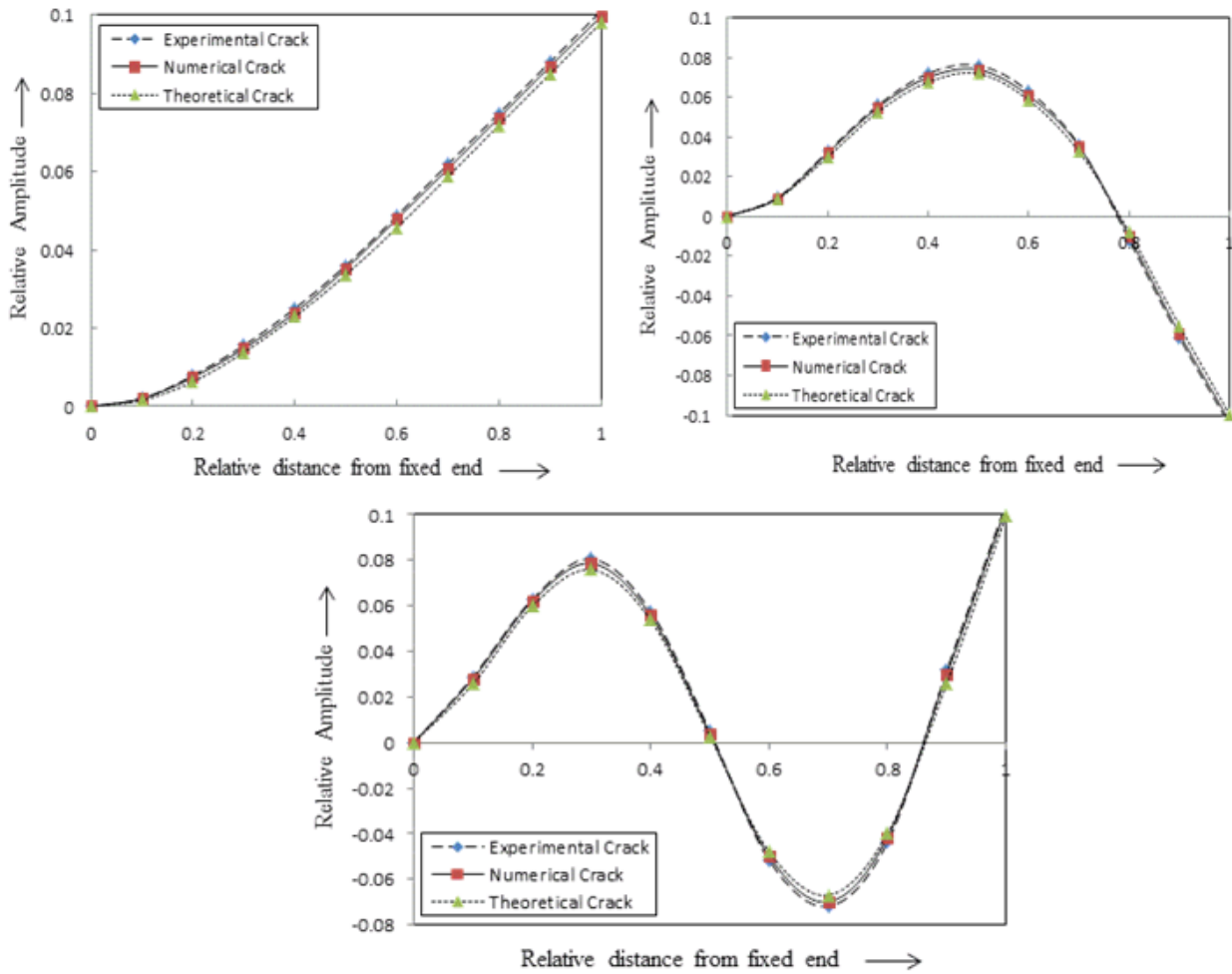
Figure 16. a Relative Amplitude vs. Relative distance from fixed end (1st mode of vibration); **b** Relative Amplitude vs. Relative distance from fixed end (2nd mode of vibration); **c** Relative Amplitude vs. Relative distance from fixed end (3rd mode of vibration)

6. Discussions

In this section a brief summary of the present work, different parameters and various methodologies used for cracks identification of composite beam are depicted below.

In this section a discussion over the results, obtained from the various methodologies used for cracks identification of composite beam are depicted below.

The nodal displacement in an element of composite beam with the orientation of the fibers and its cross sectional view is shown in Figure 1. Three nodes considered in an element, two nodes at the extreme end and one node at the middle of the element, assumed to be a node of the element having three degrees of freedom, two translations and one rotation about three mutually perpendicular axes. Two tensile loads and one moment acting on a node of the element are demonstrated in Figure 2. The relative amplitude of crack and non-crack cantilever beam for 1st, 2nd and the 3rd mode of vibration, obtained from theoretical analysis, plotted against relative distance from fixed end of cantilever beam shown in Figure 3, Figure 4 and Figure 5. The relative amplitude of the crack beam is slightly higher than non-crack, because of cracks, reducing mass and stiffness of the beam. It is observed through the magnified views at the crack locations (with =0.125 and =0.25) that there are reasonable changes in mode shapes due to the presence of crack with higher

intensity of the beam (Figure 3, Figure 4 and Figure 5). Moreover, these changes in mode shapes are more prominent at the second crack position and for the higher mode of vibration. The geometry of the cantilever composite beam with cracks is shown in Figure 6. The Geometry of Structural Solid Shell (SOLSH190) element, the meshing at the vicinity of the crack and the layers, stacking of composite beam are shown in Figure 7, Figure 8 and Figure 9 respectively. The numerical analysis results of cracked beam and theoretical analysis results of cracked and intact, presented in Figure 10, for comparison purpose. The individual material properties of fiber and matrix are listed in Table 1. The fuzzy linguistic terms and twenty five fuzzy rules out of several hundred are presented in Table 2 and Table 3 respectively. The fuzzy Gaussian membership function and fuzzy inference system with six input parameter e.g. three relative natural frequencies and three relative mode shape difference and four outputs e.g. two relative crack locations and two relative crack depths shown in Figure 11 and Figure 12. The outputs from a fuzzy inference system by activating the rule 6 and rule 16 of the Table 2 using center of gravity method are presented in Figure 14. The authentication of various analysis results, an experimental setup is fabricated shown in Figure 15. Experimental analysis results with various analysis results are presented in figure 16. A comparison of theoretical, numerical, fuzzy and experimental analysis results for cracked composite beam is in Table 4. To the different set of first three relative natural frequencies and

first three mode shapes, relative first and second crack locations and depths are compared together which outcome of various proposed methods. It is observed that the fuzzy results are more close to experimental results. The detail description of Instruments used in experimental analysis is listed in Table 5.

Table 4. Comparison of the results between Fuzzy controller, Theoretical, Numerical and Experimental analysis

Relative 1st natural frequency "rfnf"	Relative 2nd natural frequency "rsnf"	Relative 3rd natural frequency "rtnf"	Average relative 1st mode shape difference "rfmd"	Average relative 2nd mode shape difference "rsmd"	Average relative 3rd mode shape difference "rtmd"	Fuzzy controller relative 1st crack location "rfcl" 1st crack depth "rfcd" 2nd crack location "rscl" 2nd crack depth "rscd"				Theoretical relative 1st crack location "rfcl" 1st crack depth "rfcd" 2nd crack location "rscl" 2nd crack depth "rscd"			
						rfcl	rfcd	rscl	rscd	rfcl	rfcd	rscl	rscd
0.99607	0.99700	0.99829	0.000131	0.002025	0.002401	0.186	0.167	0.438	0.251	0.190	0.169	0.440	0.253
0.98098	0.99557	0.99892	0.002745	0.004556	0.010636	0.126	0.415	0.881	0.335	0.129	0.419	0.882	0.336
0.99651	0.99425	0.99796	0.000786	0.002644	0.001004	0.316	0.166	0.511	0.251	0.320	0.169	0.513	0.254
0.99001	0.99318	0.98710	0.001452	0.005709	0.005084	0.253	0.416	0.561	0.165	0.255	0.419	0.566	0.169
0.98809	0.98584	0.98255	0.002876	0.012103	0.013515	0.381	0.511	0.750	0.251	0.381	0.515	0.754	0.255
0.99672	0.98724	0.99719	0.001761	0.003319	0.005937	0.435	0.250	0.568	0.334	0.441	0.252	0.566	0.337
0.99788	0.97843	0.97519	0.002839	0.012215	0.023485	0.565	0.336	0.678	0.505	0.565	0.338	0.689	0.509
0.99874	0.99877	0.99628	0.000262	0.004753	0.015194	0.627	0.083	0.870	0.414	0.631	0.086	0.871	0.419
0.99114	0.99799	0.99803	0.000103	0.001659	0.001829	0.185	0.251	0.311	0.252	0.189	0.254	0.315	0.254
0.99701	0.98999	0.99803	0.001527	0.004641	0.002392	0.434	0.332	0.565	0.166	0.442	0.338	0.569	0.169

Relative 1st natural frequency "rfnf"	Relative 2nd natural frequency "rsnf"	Relative 3rd natural frequency "rtnf"	Average relative 1st mode shape difference "rfmd"	Average relative 2nd mode shape difference "rsmd"	Average relative 3rd mode shape difference "rtmd"	Numerical relative 1st crack location "rfcl" 1st crack depth "rfcd" 2nd crack location "rscl" 2nd crack depth "rscd"				Experimental relative 1st crack location "rfcl" 1st crack depth "rfcd" 2nd crack location "rscl" 2nd crack depth "rscd"			
						rfcl	rfcd	rscl	rscd	rfcl	rfcd	rscl	rscd
0.99607	0.99700	0.99829	0.000131	0.002025	0.002401	0.189	0.165	0.438	0.251	0.1875	0.1667	0.4375	0.250
0.98098	0.99557	0.99892	0.002745	0.004556	0.010636	0.126	0.417	0.879	0.334	0.125	0.4167	0.8750	0.333
0.99651	0.99425	0.99796	0.000786	0.002644	0.001004	0.313	0.168	0.511	0.251	0.3125	0.1667	0.5000	0.250
0.99001	0.99318	0.98710	0.001452	0.005709	0.005084	0.253	0.417	0.563	0.167	0.250	0.4167	0.5625	0.1667
0.98809	0.98584	0.98255	0.002876	0.012103	0.013515	0.376	0.510	0.752	0.253	0.375	0.5000	0.750	0.250
0.99672	0.98724	0.99719	0.001761	0.003319	0.005937	0.438	0.249	0.564	0.334	0.4375	0.2500	0.5625	0.333
0.99788	0.97843	0.97519	0.002839	0.012215	0.023485	0.563	0.335	0.688	0.503	0.5625	0.333	0.6875	0.500
0.99874	0.99877	0.99628	0.000262	0.004753	0.015194	0.628	0.084	0.869	0.417	0.625	0.0833	0.875	0.4167
0.99114	0.99799	0.99803	0.000103	0.001659	0.001829	0.188	0.251	0.311	0.252	0.1875	0.250	0.3125	0.250
0.99701	0.98999	0.99803	0.001527	0.004641	0.002392	0.438	0.335	0.564	0.168	0.4375	0.333	0.5625	0.1667

Table 5. Decription of Instruments used in experimental analysis

S No	Name of the Instrument	Description of Instruments
1	**Vibration Analyzer**	Product Name :Pocket front end Product Type :3560L Manufacturer Bruel & kjaer Frequency Range :7 Hz to 20 Khz Channels :2 Inputs, 2 Tachometer Input Type:Direct/CCLD
2	**Delta Tron Accelerometer**	Manufacture Bruel & kjaer Product Type : 4513-001 Sensitivity :10mv/g-500mv/g Frequency Range :1Hz-10KHz Supply voltage : 24volts Operating temperature Range : -50^{0}C to +100^{0}c
3	**Vibration indicator**	PULSE LabShop Software Version 12 Manufacture :Bruel & kjaer
4	**Vibration Exciter**	Product Type :4808 Permanent Magnetic Vibration Exciter Force rating 112N (25 lbf) sine peak (187 N (42 lbf) with cooling) Manufacture :Bruel & kjaer Frequency Range : 5Hz to 10 kHz First axial resonance : 10 kHz Maximum bare table Acceleration :700 m/s2 (71 g)
5	**Power Amplifier**	ProductType : 2719 Manufacture :Bruel & kjaer Power Amplifier :180VA
6	**Test specimen**	Double crack cantilever composite beam with dimension 800mmx50mmx6mm
7	**Power Distribution**	220V power supply, 50Hz
8	**Function Generator**	Product Model :FG200K Manufacturer : Aplab Frequency Rang :0.2Hz to 200 KHz VCG IN connector for Sweep Generation Sine, Triangle, Square, TTL outputs Output Level 15Vp-p into 600 ohms Rise/Fall Time : <300nSec:

7. Conclusions

The following conclusions derived from the various studies as mentioned above are described below

1. In the present work, theoretical, numerical, experimental and fuzzy logic technique has been adopted for the identification of cracks of the beam like dynamic structure.

2. Online fuzzy controller is developed based on Gaussian membership function, relative first three natural frequencies and relative first three mode shape difference used as input parameters and outputs are relative crack location and relative crack depth.

3. Theoretical and numerical analysis is performed to get modal parameters such as natural frequencies and mode shapes of cracked and non-cracked cantilever composite beam.

4. An experimental setup is established to validate the results, obtained from various discussed methods. Results of experimental analysis for faulty dynamic beam structures are in good agreement with theoretical, numerical and fuzzy analysis results. It is observed that fuzzy results are more closed to experimental results.

5. This online fuzzy inverse technique can be used for health monitoring of structures and mechanical system, which reduced computational and damage detection time.

References

[1] Kisa M (2004) Free vibration analysis of a cantilever composite beam with multiple cracks, *Composites Science and Technology,* 64, 1391-1402.

[2] Kisa M and Gurel MA (2006) Modal analysis of multi-cracked beamswith circular cross section, *Engineering Fracture Mechanics,* 73, 963-977.

[3] Krawczuk M and Ostachowicz WM (2005) Modelling and vibration analysis of acantilever composite beam with atransverse open crack, *Journal of Sound and Vibration,* 183(1), 69-89.

[4] Hoffman AJandVan der Merwe NT (2002) The application of neural networks to vibrational diagnostics for multiple fault conditions", *Computer Standards & Interfaces,* 24,139-149.

[5] Adams RD, CawleyP, PyeCJ and Stone J (1978). A vibration testing fornon-destructively assessing the integrity of the structures,*Journal of Mechanical Engineering Science,* 20,93-100.

[6] SekharAS (1998) Vibration characteristics of a cracked rotor with twoopen cracks, *Journal of Sound and Vibration,* 223(4), 497-512.

[7] Pawar PM and Ganguli R (2007) Genetic fuzzy system for online structural health monitoring of composite helicopter rotor blades, *Mechanical Systems and Signal Processing,* 21, 2212-2236.

[8] Katunin A (2010) Identification of multiple cracks in composite beams using discrete wavelet transform, *Scientific Problems of Machines Operation and Maintenance,* 2 (162), 42-52.

[9] SaravananN, Cholairajan S, and Ramachandran KI (2009) Vibration based fault diagnosis of spur, bevel gear box using fuzzy technique, *Epert System with Applications,* 36, 3119-3135.

[10] Das AK and Parhi DRK (2011) Development of an inverse methodology for crack diagnosis using AI technique, *International Journal Computational Material Science and Surface Engineering,* 4(2), 143-167.

[11] Parhi DRK (2005) Navigation of Mobile root using a fuzzy logic controller, *Journal intelligent and robotics systems: Theory and Applications,* 42, 253-273.

[12] Mohammed RS and Kapania RK. (2013) Damage Detection in a Prestressed membrane using a wavelet-based Neuro-fuzzy System, *AIAA Journal,* 51(11), 2558-2569.

[13] Nikpour K and Dimarogonas AD (1988) Local compliance of composite cracked bodies, *Composite Science and Technology,* 32,209-223.

[14] Bao G, FanB, HoS and SuoZ (1992) The role of material orthotropy infracture specimens for composites" *International Journalof Solids Structures,* 29, 1105-1116.

[15] Nikpour K. (1990). Buckling of cracked composite columns, *International J Solids Structure,* 26(12), 1371-1386.

[16] TadaH, Paris PC And IrwinGR (1985) *The stress analysis of cracks handbook 2nd ed. St. Louis,* MO: Paris production incorporated and Del Research Corporation.

[17] PrzemienieckiJS (1967) *Theory of matrix structural analysis. 1st edition.* London: McGraw-Hill.

[18] VinsonJR, and SierakowskiRL (1991) *Behaviour of structures composed of composite materials. 1st edition.* Dordrecht: Martinus Nijhoff, 1991.

Appendix A

Where q_{ij} (i, j=1… 9) are given as

$q_{11} = q_{77} = 7BH\bar{Q}_{11}/3L_e,$

$q_{12} = q_{21} = -q_{78} = -q_{87} = 7BH\bar{Q}_{13}/3L_e,$

$q_{13} = q_{31} = -q_{79} = -q_{97} = BH\bar{Q}_{13}/2_e,$

$q_{47} = q_{74} = -q_{14} = -q_{41} = 8BH\bar{Q}_{11}/3L_e,$

$q_{15} = -q_{51} = -q_{42} = q_{24} = -q_{48} = -q_{84} = -q_{57} = -q_{75} = 8BH\bar{Q}_{13}/3L_e,$

$q_{16} = q_{61} = -q_{34} = -q_{43} = q_{49} = q_{94} = -q_{67} = -q_{76} = 2BH\bar{Q}_{13}/3,$

$q_{17} = q_{71} = BH\bar{Q}_{11}/3L_e$

$q_{18} = q_{81} = q_{27} = q_{72} = BH\bar{Q}_{13}/3L_e$

$q_{73} = q_{37} = -q_{19} = -q_{91} = BH\bar{Q}_{13}/6,$

$q_{22} = q_{88} = 7BH\bar{Q}_{11}/3L_e$

$q_{23} = q_{32} = -q_{89} = -q_{98} = BH\bar{Q}_{13}/2,$

$q_{25} = q_{52} = -q_{58} = -q_{85} = -8BH\bar{Q}_{33}/3L_e,$

$q_{26} = q_{62} = q_{59} = q_{95} = -q_{53} = q_{35} = -q_{86} = -q_{68} = 2BH\bar{Q}_{33}/3,$

$q_{28} = q_{82} = BH\bar{Q}_{33}/3L_e,$

$q_{38} = q_{83} = -q_{29} = -q_{92} = BH\bar{Q}_{33}/6,$

$q_{45} = q_{54} = 16BH\bar{Q}_{13}/3L_e,$

$q_{44} = 16BH\bar{Q}_{11}/3L_e,$

$q_{55} = 16BH\bar{Q}_{33}/3L_e,$

$q_{33} = q_{99} = BH(7H^2\bar{Q}_{11}/36L_e + L_e\bar{Q}_{33}/9),$

$q_{36} = q_{63} = q_{69} = q_{96} = BH(-2H^2\bar{Q}_{11}/9L_e + L_e\bar{Q}_{33}/9),$

$q_{39} = q_{93} = BH(H^2\bar{Q}_{11}/36L_e - L_e\bar{Q}_{33}/18),$

$q_{66} = BH(4H^2\bar{Q}_{11}/9L_e + 4L_e\bar{Q}_{33}/9),$

$q_{46} = q_{56} = 0,$

Where B, H, L_e are the geometrical parameters of the composite beam element, $\bar{Q}_{11}$, $\bar{Q}_{13}$ and $\bar{Q}_{33}$ are stress-stress constants and given as [18]

$\bar{Q}_{11} = \bar{C}_{11}m^4 + 2(\bar{C}_{12} + 2\bar{C}_{33})m^2n^2 + \bar{C}_{22}n^4,$

$\bar{Q}_{13} = (\bar{C}_{11} - \bar{C}_{12} - 4\bar{C}_{33})m^3n + \bar{C}_{12} - \bar{C}_{22} - 2\bar{C}_{33}mn^3$

$\bar{Q}_{33} = (\bar{C}_{11} - 2\bar{C}_{12} + \bar{C}_{22} - 2\bar{C}_{33})m^2n^2 + \bar{C}_{33}(m^4 + n^4),$

Where m=cosα, n=sinα and C_{ij} terms are determined from the relation [15]

$\bar{C}_{11} = \dfrac{E_{11}}{(1-v_{23}^2E_{22}/E_{11})},$

$\bar{C}_{22} = \bar{C}_{11}E_{22}/E_{11},$

$\bar{C}_{12} = v_{12}\bar{C}_{22}, \quad \bar{S}_{33} = G_{12}$

Where E_{11}, E_{22}, G_{12}, G_{23}, υ_{12}, v_{23} and ρ are the mechanical properties of the composite and calculated using the following formulae [18]:

$E_{11} = E_f\varphi + E_m(1-\varphi),$

$E_{22} = E_m\left[\dfrac{E_f + E_m + (E_f - E_m)\varphi}{E_f + E_m - (E_f - E_m)\varphi}\right],$

$v_{12} = v_f\varphi + v_m(1-\varphi),$

$v_{23} = v_f\varphi + v_m(1-\varphi)\left[\dfrac{1 + v_m - v_{12}E_m/E_{11}}{1 - v_m^2 + v_mv_{12}E_m/E_{11}}\right],$

$G_{12} = G_m\left[\dfrac{G_f + G_m + (G_f - G_m)\varphi}{G_f + G_m - (G_f - G_m)\varphi}\right],$

$\rho = \rho_f\varphi + \rho_m(1-\varphi),$

$G_{23} = \dfrac{E_{22}}{2(1+v_{23})},$

Where, m and f denote matrix and fiber, respectively. E, G, v and ρ are the modulus of elasticity, the modulus of rigidity, the Poisson's ratio and the mass density respectively.

Appendix B

Where M_{ij} (i, j=1… 9) are given as

$m_{11} = m_{22} = m_{77} = m_{88} = m_{14} = m_{41} = 2\rho BHL_e/15,$

$m_{17} = m_{71} = m_{28} = m_{82} = -\rho BHL_e/30,$

$m_{23} = m_{32} = -m_{38} = -m_{83} = -m_{89} = -m_{98} = \rho BHL_e^2/180,$

$m_{68} = m_{86} = -m_{26} = -m_{62} = \rho BHL_e^2/90,$

$m_{33} = m_{99} = \rho BHL_e(L_e^2/1890 + H^2/90),$

$m_{66} = 2\rho BHL_e(L_e^2/1890 + H^2/90),$

$$m_{36} = m_{63} = m_{69} = m_{96} = \rho BHL_e(-L_e^2/945 + H^2/180),$$

$$m_{39} = m_{93} = \rho BHL_e(L_e^2/1890 - H^2/90),$$

$$m_{44} = m_{55} = 8\rho BHL_e/15,$$

$$m_{12} = m_{21} = m_{13} = m_{31} = m_{15} = m_{51} = m_{16} = m_{61} = m_{18} = m_{81} = m_{19} = m_{91}$$

$$= m_{24} = m_{42} = m_{27} = m_{72} = m_{34} = m_{43} = m_{35} = m_{53} = m_{37} = m_{73} = m_{45} = m_{54}$$

$$= m_{46} = m_{64} = m_{48} = m_{84} = m_{49} = m_{94} = m_{56} = m_{65} = m_{57} = m_{75} = m_{59} = m_{95}$$

$$= m_{67} = m_{76} = m_{78} = m_{87} = m_{79} = m_{97} = 0$$

Where ρ is the mass density of the element, B is the width of the element, H is the height of the element and L_e denotes the length of the element.

Appendix C

The roots of the follow characteristic equation give the complex constants s_1 and s_2 [18]:

$$\bar{d}_{11}s^4 - 2\bar{d}_{16}s^3 + (2\bar{d}_{12} + \bar{d}_{66})s^2 - 2\bar{d}_{26}s + \bar{d}_{22} = 0,$$

Where $\bar{d}_{ij}$ constants are

$$\bar{d}_{11} = d_{11}m^4 + (2d_{12} + d_{66})m^2n^2 + d_{22}n^4,$$

$$\bar{d}_{22} = d_{11}n^4 + (2d_{12} + d_{66})m^2n^2 + d_{22}m^4,$$

$$\bar{b}_{12} = (d_{11} + d_{22} - d_{66})m^2n^2 + d_{12}(m^4 + n^4),$$

$$\bar{d}_{16} = (-2d_{11} + 2d_{12} + d_{66})m^3n + (d_{22} - 2d_{12} - d_{66})mn^3,$$

$$\bar{d}_{26} = (-2d_{11} + 2d_{12} + d_{66})mn^3 + (d_{22} - 2d_{12} - d_{66})m^3n,$$

$$\bar{d}_{66} = 2(2d_{11} - 4d_{12} + 2d_{22} - d_{66})n^2m^2 + d_{66}(m^4 + n^4),$$

Where $m = \cos\alpha$ $n = \sin\alpha$ and $\bar{d}_{ij}$ are compliance constants of the campsite along the principal axes. $\bar{d}_{ij}$ can be related to the mechanical constants of the material by

$$d_{11} = \frac{1}{E_{11}}(1 - v_{12}^2\frac{E_{22}}{E_{11}}), d_{22} = \frac{1}{E_{22}}(1 - v_{23}^2), d_{12} = \frac{-v_{12}}{E_{11}}(1 + v_{23}), d_{66} = 1/G_{12}, d_{44} = 1/G_{23}, d_{55} = d_{66}.$$